PLOS ONE

RESEARCH ARTICLE

Distributions of Direct, Reflected, and Diffuse Irradiance for Ocular UV Exposure at Different Solar Elevation Angles

Jiaming Yu[1], Hui Hua[2], Yan Liu[3], Yang Liu[2]*

1 Ophthalmology Department, the Fourth Affiliated Hospital of China Medical University, Shenyang, Liaoning, China, **2** School of Public Health, China Medical University, Shenyang, Liaoning, China, **3** Department of Biomedical Engineering, China Medical University, Shenyang, China

* yangliu@cmu.edu.cn

Citation: Yu J, Hua H, Liu Y, Liu Y (2016) Distributions of Direct, Reflected, and Diffuse Irradiance for Ocular UV Exposure at Different Solar Elevation Angles. PLoS ONE 11(11): e0166729. doi:10.1371/journal.pone.0166729

Editor: Ganesh Chandra Jagetia, Mizoram University, INDIA

Received: June 3, 2016

Accepted: November 2, 2016

Published: November 15, 2016

Data Availability Statement: All relevant data are within the paper and its Supporting Information files.

Funding: This work was supported by the National Natural Science Foundation of China, Grant NO:81273034 (https://isisn.nsfc.gov.cn/egrantindex/funcindex/prjsearch-list) to YL and the Natural Science Foundation of Liaoning Province, China, Grant No: 2014021009 (http://kjjh.lninfo.gov.cn/) to JMY. The funders had no role in study design, data collection and analysis, decision to publish, or preparation of the manuscript.

Abstract

To analyze intensities of ocular exposure to direct ($E_{o,dir}$), reflected ($E_{o,refl}$), and diffuse ($E_{o,diff}$) ultraviolet (UV) irradiance at different solar elevation angles (SEAs), a rotating manikin and dual-detector spectrometer were used to monitor the intensity of ocular exposure to UV irradiation (E_o) and ambient UV radiation (UVR) under clear skies in Sanya, China. $E_{o,dir}$ was derived as the difference between maximum and minimum measured E_o values. $E_{o,refl}$ was converted from the value measured at a height of 160 cm. $E_{o,diff}$ was calculated as the minimum measured E_o value minus $E_{o,refl}$. Regression curves were fitted to determine distributions of intensities and growth rates at different wavelengths and SEAs. $E_{o,dir}$ differed from ambient UVR exposure. Linear, quadratic, and linear $E_{o,dir}$ distributions were obtained in SEA ranges of 14˚–30˚, 30˚–50˚, and 50˚–90˚, respectively, with maximum $E_{o,dir}$ at 32˚–38˚ SEA. Growth rates of $E_{o,dir}$ with increasing wavelength were fitted with quadratic functions in all SEA ranges. Distributions and growth rate of $E_{o,refl}$ values were fitted with quadratic functions. Maximum $E_{o,diff}$ was achieved at the same SEA for all fitted quadratic functions. Growth rate of $E_{o,diff}$ with increasing wavelength was fitted with a linear function. $E_{o,dir}$ distributions were fitted with linear or quadratic functions in different SEA ranges. All $E_{o,refl}$ and $E_{o,diff}$ distributions were fitted with quadratic functions. As SEA increased, the $E_{o,dir}$ portion of E_o increased and then decreased; the $E_{o,refl}$ portion increased from an initial minimum; and the $E_{o,diff}$ portion first decreased and then increased. The findings may provide data supporting on construction of a mathematical model of ocular UV exposure.

Introduction

Ultraviolet (UV) radiation (UVR) has harmful effects on humans, causing damage to the ocular lens, cornea, and retina [1–3]. Any estimation of the risk of ocular UV damage should include an evaluation of the intensity of ocular exposure to UV irradiation (E_o). Effects of UVR exposure have been studied in animals, provided important preliminary data [4–6], as well as in human subjects wearing UVR dose detectors [7]. For instance, UVR exposure across the corneal surface was measured in subjects wearing polysulfone contact lenses while walking on a grass field on a cloudy day [8]. In another study, UVR-sensitive films were placed on

Competing Interests: The authors have declared that no competing interests exist.

subjects' hats, glasses, and chins to evaluate ocular exposure to UV irradiation [9]. Field-based UVR sensors placed on the human body have been used to measure ocular exposure to UV irradiation for a range of solar elevation angles (SEAs), ambient conditions, and head orientations [10]. Manikins have also been used to simulate ocular UV exposure for humans [11, 12].

Ultraviolet (UV) radiation dose has been estimated by using mathematical models, based on data from environmental monitoring, ozone layer thickness, aerosol, cloud thickness, and other parameters. Models have been used to calculate intensities of direct, diffuse, and reflected solar UV irradiance on the horizontal, vertical, and inclined planes [13–22] or in the environment [23, 24]. Researchers have utilized three-dimensional digital models or different body position models to simulate UV exposure [16, 25, 26]. However, because of the complexity of ocular anatomy, monitoring instruments cannot be used to measure directly the intensities of ocular exposure to direct ($E_{o,dir}$), reflected ($E_{o,refl}$) or diffuse ($E_{o,diff}$) UV irradiance.

Previous studies of ocular exposure to UV irradiance have concentrated on monitoring the ocular UV exposure state. To the best of our knowledge, no study has described splitting ocular exposure to UV irradiation into components of direct, reflected, and diffuse UV irradiance. We previously analyzed ocular exposure to UVR at different wavelengths, azimuths, orientations, and reflected backgrounds [10, 11, 27, 28]. We determined that ocular exposure to direct, reflected, and diffuse UV irradiance can be regarded as basic parameters for constructing a mathematical model of ocular UV exposure, which could be used to calculate and compare ocular UV exposure in different regions.

The present study was conducted to monitor the direct, reflected, and diffuse components of ocular exposure to UV irradiation using our self-made ocular UV exposure model. Distributions of ocular exposure to direct, reflected, and diffuse UV irradiance on a rotating manikin were analyzed for different UVR wavelengths and solar elevation angles during the daytime under fine weather in Sanya, China. The goal was to determine the times of maximum ocular exposure to UV irradiation, enabling the prevention of ocular injury from solar UV. Moreover, the findings will provide important data supporting the construction of a mathematical model of ocular UV exposure.

Material and Methods

Experimental apparatus

The experimental apparatus was a rotating manikin, which comprised a turntable base, shelf, and anthropomorphic model with realistic facial features (Fig 1). The eye level was at a height of approximately 160 cm. The chosen solar UV sensor, a dual-channel miniature fiber optic spectrometer (AvaSpec-2048x14-2-USB2, Netherlands) with two detectors, was placed on the shelf. One detector was mounted on a plane tangent to the position of the right cornea at the most anterior point on the manikin to record ocular UV exposure (Fig 1A). The other was placed at the vertex of the head of the manikin to record ambient UV irradiance. The visual line was approximately 10˚ below the horizontal (Fig 1B). The field of view of the manikin was approximately 139˚, due to the forehead and malar (Fig 1B). Ground reflection data were obtained with the monitoring instrument at a height of 160 cm and facing the ground. Spectrometer and other equipment were calibrated by the National Physical Laboratory GB before the experiment, as described previously [11].

Study location

The study site was located in the town of Hai Tang Wan in Sanya city (8.4˚ N, 109.7˚ E, altitude 18 m) in the province of Hainan, China. Sanya is the southernmost city in Hainan Island, which has a maximum SEA of nearly 90˚ in July. The experimental apparatus was located on

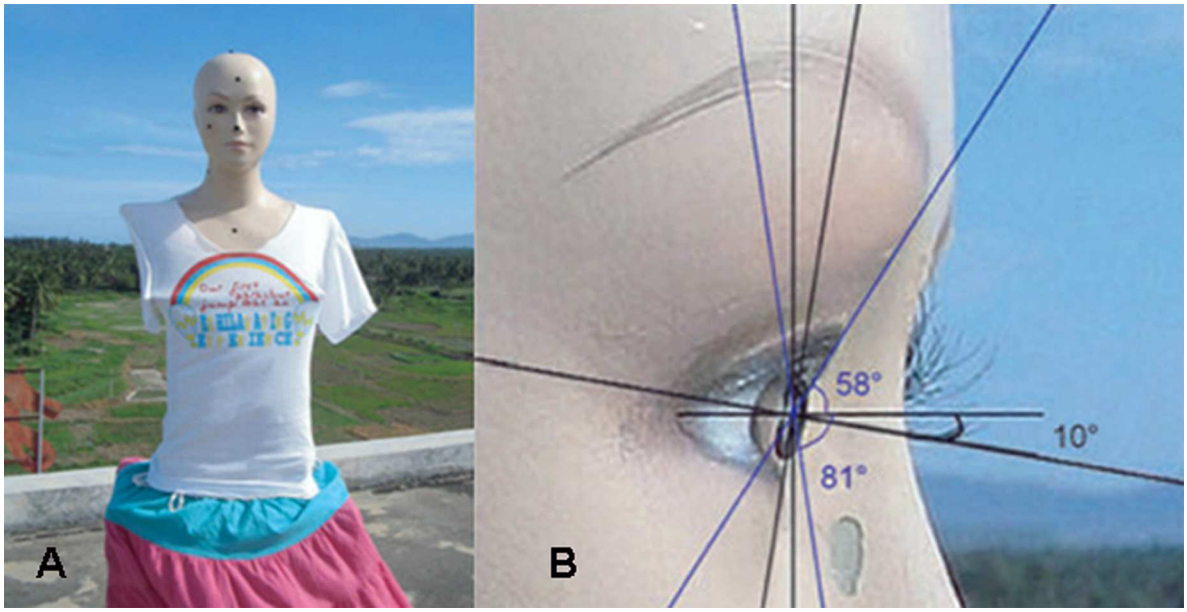

Fig 1. (A) Rotating manikin with solar UV sensor. (B) Details of manikin.

doi:10.1371/journal.pone.0166729.g001

the asphalt-covered concrete roof of a five-story hotel surrounded by grass with an unobstructed view. The owner of this hotel called "Dingjun Xu" permitted us to carry out measurements on the roof of his hotel.

Meteorological conditions

Measurements of UV irradiance exposure were conducted on July 11, 2010 from 08:00 to 19:00 China Standard Time (CST) (solar noon at about 12:55 CST). This day was a sunny day and clear sky.

UV irradiance measurements

The manikin was rotated clockwise at a constant speed during data collection, beginning with the position of facing the sun. UV irradiance can be monitored (unit $\mu W\ cm^{-2}\ nm^{-1}$) was calculated in 1-s intervals from the integration of the UVA band (320–400 nm) and UVB band (300–320 nm). Duration of each measurement progression was 1 min, and the measurement interval was 5 min. There were 60 groups of irradiance data per manikin revolution. The maximum E_o at different wavelengths of each revolution was calculated to simulate the actual maximum UVR exposure under clear skies. The same procedure was used simultaneously to obtain data from the ambient detector.

Definitions

$E_{o,dir}$ referred to UV irradiation received by the probe placed at the eye position of monitoring model, which consisted of direct solar UV irradiation going straight into the eyes at a certain range of SEAs and/or refraction from direct solar UV hitting the facial structure. $E_{o,dir}$ was measured as the difference between the maximum and minimum values of E_o measured from the instrument. Intensity of UV irradiance measured by the equipment at a height of 160 cm

was converted to $E_{o,refl}$, according to the structure of the human eye, using the formula [29]:

$$I_{r,\lambda} = 0.5S(\lambda)(1 - \cos 100^{\circ})$$

where S(λ) is the measured spectral irradiance. $E_{o,diff}$ was calculated as the difference between the minimum value of measured ocular UV exposure and $E_{o,refl}$.

Data calculation

Data from the spectrometer were processed with AvaSoft 7.4 USB2.0. Ocular UV exposure and ambient UV data were processed separately. Maximum and minimum integrated E_o values of each revolution were calculated from the actual maximum and minimum UV exposures under clear skies. Ocular UV exposure data obtained from the position of the model facing the sun were used to simulate the maximum E_o value. When the manikin had its back towards the sun, E_o had only reflected and diffuse irradiance dimensions. Data obtained in this position were used as the minimum E_o values.

Monitoring time and SEA

Monitoring time was from 08:00 CST (25° SEA) to 18:00 CST (14° SEA). Range of SEAs was from 14° to 90°, with maximum SEA occurring at about 12:40 CST. According to the relationship between monitoring time and SEA, E_o was measured in three ranges of SEA: $14^{\circ} < SEA \leq 30^{\circ}$ (low), $30^{\circ} < SEA \leq 50^{\circ}$ (middle) and $50^{\circ} < SEA \leq 90^{\circ}$ (high).

Results

Ambient and ocular UV irradiance at different SEAs

Fig 2 shows the distributions of ambient and ocular UV irradiance intensities at different SEAs. Maximum UV irradiance at each SEA was used as the intensity of ambient UV irradiance (E_{amb}). Total E_o was determined at nine representative wavelengths of the 300–400 nm UV spectral range, including five wavelengths in the 300–320 nm range (300, 305, 310, 315, and 320 nm) and four wavelengths in the 325–400 nm range (325, 350, 375, and 399 nm).

E_{amb} increased with increasing SEA, with maximum E_{amb} being measured at the highest SEA (Fig 2A). Maximum E_o with different wavelengths was achieved in the 30°–40° SEA range (Fig 2B).

Distributions and growth rates of $E_{o,dir}$ at selected wavelengths and different SEAs

$E_{o,dir}$ distributions at different SEAs differed markedly from the E_{amb} distribution (Fig 3). In the low range (14°–30° SEA), $E_{o,dir}$ values at different wavelengths increased with increasing SEA, and the distributions were fitted with linear functions (Fig 3D). In the middle range (30°–50° SEA), $E_{o,dir}$ showed binomial distributions, first increasing and then decreasing with SEA, peaking at about 32–38° SEA (Fig 3E). These distributions were fitted with quadratic functions. As wavelength increased in the middle SEA range, the opening of the curve of the quadratic function gradually decreased. In the high range (50°–90° SEA), $E_{o,dir}$ distributions were largely parallel to the x-axis and constant with increasing SEA from 300 to 310 nm, but decreased with increasing SEA from 310 to 400 nm. $E_{o,dir}$ distributions were fitted with linear functions (Fig 3F). For a given SEA, $E_{o,dir}$ increased with increasing wavelength. Equations for regression curves fitted to the $E_{o,dir}$ distributions with increasing SEA are given in Table 1.

To describe the growth rates of $E_{o,dir}$ values with increasing wavelength, coefficients of each fitted equation in Table 1 were used to fit curves with different wavelengths (Fig 4). In the low

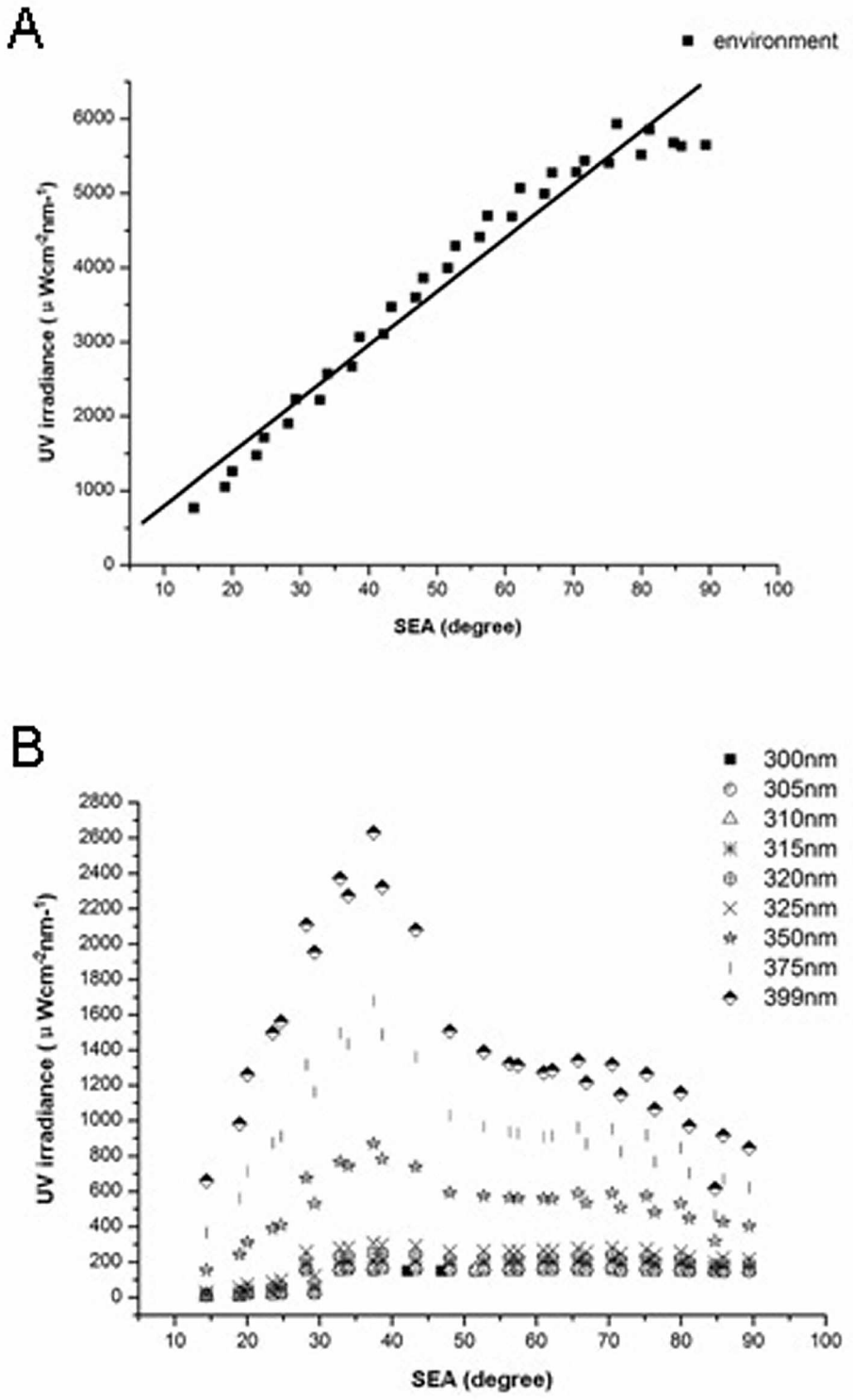

Fig 2. (A) Ambient UV irradiance at different solar elevation angles and fitted regression curve. (B) Ocular UV irradiance of selected wavelengths at different solar elevation angles.

doi:10.1371/journal.pone.0166729.g002

SEA range (Fig 4A), the curve slope (gradient) of each linear equation increased with increasing wavelength. The growth rate of curve slopes was fitted with a quadratic function ($y = 0.008x2–5.324x + 813.7$; $R^2 = 0.999$). In the middle SEA range (Fig 4B), binomial

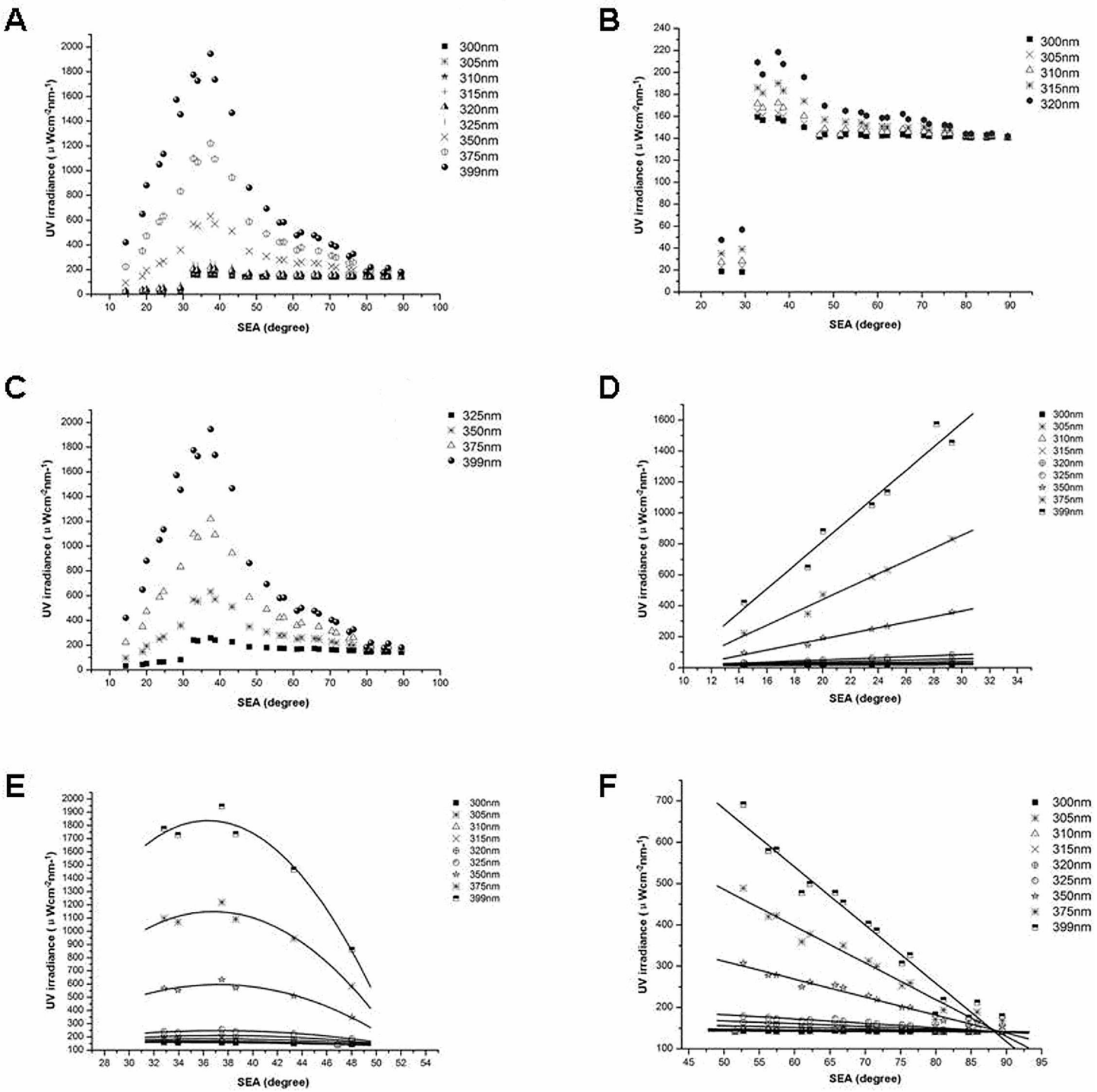

Fig 3. Distributions of intensities and fitted regression curves for ocular exposure to direct UV irradiance of selected wavelengths at different solar elevation angles. (A-C) Intensity distributions at different SEAs for UVR of 300–399 nm (A), 300–320 nm (B), and 325–399 (C). (D-F) Fitted regression curves for all selected wavelengths at low (D), middle (E), and high solar elevation angle range (F).

doi:10.1371/journal.pone.0166729.g003

Table 1. Fitted equations for distributions of ocular exposure to direct UV irradiance of selected wavelengths.

Wavelength	14˚-30˚ SEA		30˚- 50˚ SEA		50˚- 90˚ SEA	
	Fitted equation	R^2	Fitted equation	R^2	Fitted equation	R^2
305nm	y = 0.393x+12.330	R^2 = 0.787	y = -0.095x2+6.337x+57.964	R^2 = 0.943	y = 142.869	
310nm	y = 0.595x+12.227	R^2 = 0.890	y = -0.147x2+10.174x-5.611	R^2 = 0.915	y = 144.616	
315nm	y = 1.104x+7.689	R^2 = 0.980	y = -0.211x2+15.219x-88.641	R^2 = 0.937	y = -0.376x+174.630	R^2 = 0.929
320nm	y = 2.034x-2.335	R^2 = 0.998	y = -0.361x2+26.845x-288.670	R^2 = 0.878	y = -0.672x+201.360	R^2 = 0.926
325nm	y = 3.408x-17.374	R^2 = 0.995	y = -0.526x2+39.129x-479.130	R^2 = 0.932	y = -1.055x+235.670	R^2 = 0.942
350nm	y = 17.997x-173.750	R^2 = 0.986	y = -2.135x2+158.770x-2354.500	R^2 = 0.949	y = -4.352x+529.810	R^2 = 0.958
375nm	y = 41.533x-389.790	R^2 = 0.985	y = -4.499x2+330.920x-4935.900	R^2 = 0.961	y = -8.887x+930.160	R^2 = 0.959
399nm	y = 76.526x-714.560	R^2 = 0.963	y = -7.286x2+530.170x-7806.600	R^2 = 0.968	y = -14.081x+1385.300	R^2 = 0.957

doi:10.1371/journal.pone.0166729.t001

coefficients of the fitted equations increased with increasing wavelength. The growth rate of the absolute values of the binomial coefficients was fitted with a quadratic function ($y = -0.0007x^2 + 0.390x - 57.123$; $R^2 = 0.999$). In the high SEA range (Fig 4C), the curve slope of each linear equation increased with increasing wavelength. The growth rate of the absolute values of the curve slopes was fitted with a quadratic function ($y = -0.001x^2 + 0.5227x - 69.305$; $R^2 = 0.9997$).

Distributions and growth rates of $E_{o,refl}$ at selected wavelengths and different SEAs

Distributions of $E_{o,refl}$ values at different SEAs differed from the distributions of $E_{o,dir}$ values (Fig 5). Distributions of $E_{o,refl}$ of selected wavelengths increased with increasing SEA and were fitted with quadratic functions (Table 2). The maximum value of each quadratic function increased with increasing SEA or increasing UV wavelength. Absolute values of the binomial coefficients of the fitted equations increased with increasing wavelength (Fig 6). The growth rate of these changes was fitted with a quadratic function ($y = -3E\text{-}06x^2 + 0.001x - 0.183$; $R^2 = 0.9989$). $E_{o,refl}$ increased quickly with increasing SEA or increasing wavelength. The opening of the curve of the quadratic function gradually decreased and the binomial curve become steeper with increasing SEA (Fig 5).

Distributions and growth rates of $E_{o,diff}$ at selected wavelengths and different SEAs

Distributions of $E_{o,diff}$ at different SEAs differed from $E_{o,dir}$ but were similar to $E_{o,refl}$ distributions (Fig 7). At the selected wavelengths, $E_{o,diff}$ first increased and then decreased with increasing SEA. All distributions were fitted with quadratic functions (Table 3). In contrast to $E_{o,refl}$, the maximum $E_{o,diff}$ of each fitted quadratic function with increasing wavelength was achieved at the same SEA of about 62˚. Absolute values of the binomial coefficients of each fitted equation increased with increasing wavelength (Fig 8). The growth rate with increasing wavelength was fitted with a linear function ($y = -0.0012x + 0.362$; $R^2 = 0.999$). As wavelength increased, the opening of the curve of the quadratic function decreased at a constant speed. As SEA increased, the rate of change of $E_{o,diff}$ was faster at larger wavelengths (Fig 7).

Percentages of $E_{o,dir}$, $E_{o,refl}$, and $E_{o,diff}$ in total E_o

Fig 9 shows the percentages of the total E_o due to $E_{o,dir}$, $E_{o,refl}$, and $E_{o,diff}$ at 350 nm (Fig 9A) and 399 nm (Fig 9B). As SEA increased, the relative percentages of the three components significantly differed from each other. The percentage due to $E_{o,dir}$ first increased and then

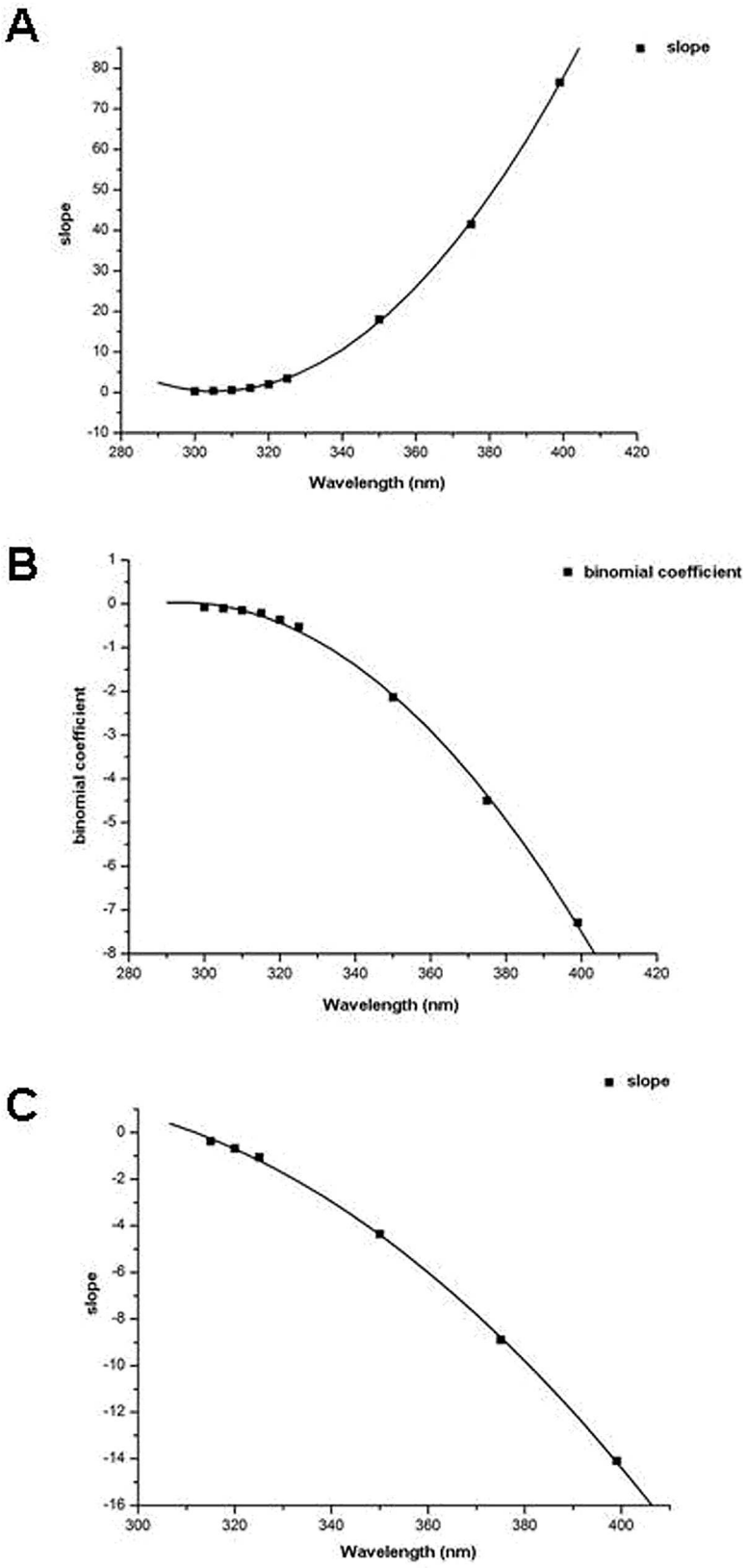

Fig 4. Growth rate of intensity of ocular exposure to direct UV irradiation with increasing wavelength and fitted regression curves in the low (A), middle (B), and high solar elevation angle range (C).

doi:10.1371/journal.pone.0166729.g004

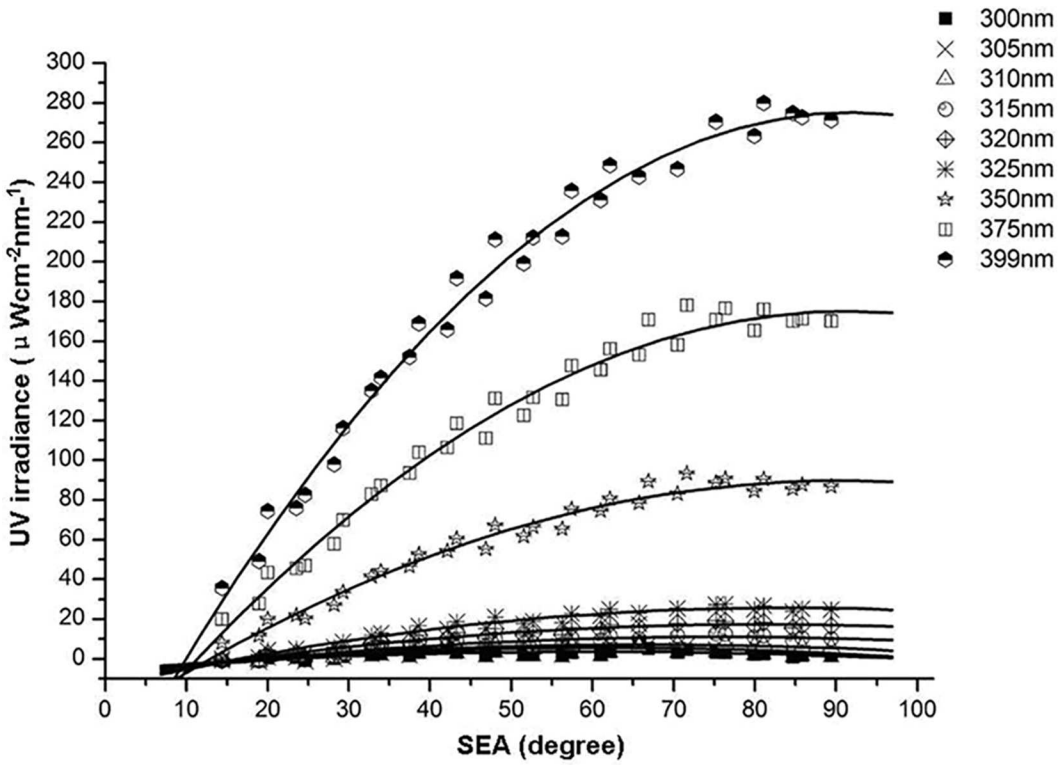

Fig 5. Distributions of intensity of ocular exposure to reflected UV irradiance of selected wavelengths at different solar elevation angles and fitted regression curves.

doi:10.1371/journal.pone.0166729.g005

decreased with increasing SEA. The percentage due to $E_{o,refl}$ gradually increased from an initial minimum. The percentage due to $E_{o,diff}$ first decreased and then increased.

Discussion

As we all known, the diurnal distribution of environmental UV exposure is a bell shaped curve, the highest ambient UV irradiances were measured at the highest solar elevation angle, the direction is the dominant in ambient UV irradiances. However, for the ocular UV irradiance, the findings in our previous studies showed the ocular UV irradiances diurnal variations

Table 2. Fitted equations for distributions of ocular exposure to reflected UV irradiance of selected wavelengths.

Wavelength (nm)	Fitted equation	R^2
305	y = -0.0029x2+ 0.346x - 5.470	R^2 = 0.949
310	y = -0.0032x2+ 0.432x - 7.254	R^2 = 0.90
315	y = -0.0034x2+ 0.522x - 8.849	R^2 = 0.901
320	y = -0.0044x2+ 0.713x - 11.383	R^2 = 0.938
325	y = -0.0056x2+ 0.948x - 14.128	R^2 = 0.957
350	y = -0.0150x2+ 2.705x - 32.464	R^2 = 0.977
375	y = -0.0273x2+ 4.992x - 53.320	R^2 = 0.983
399	y = -0.0410x2+ 7.536x - 70.992	R^2 = 0.988

Data represent results for the entire range of solar elevation angles (14–90˚).

doi:10.1371/journal.pone.0166729.t002

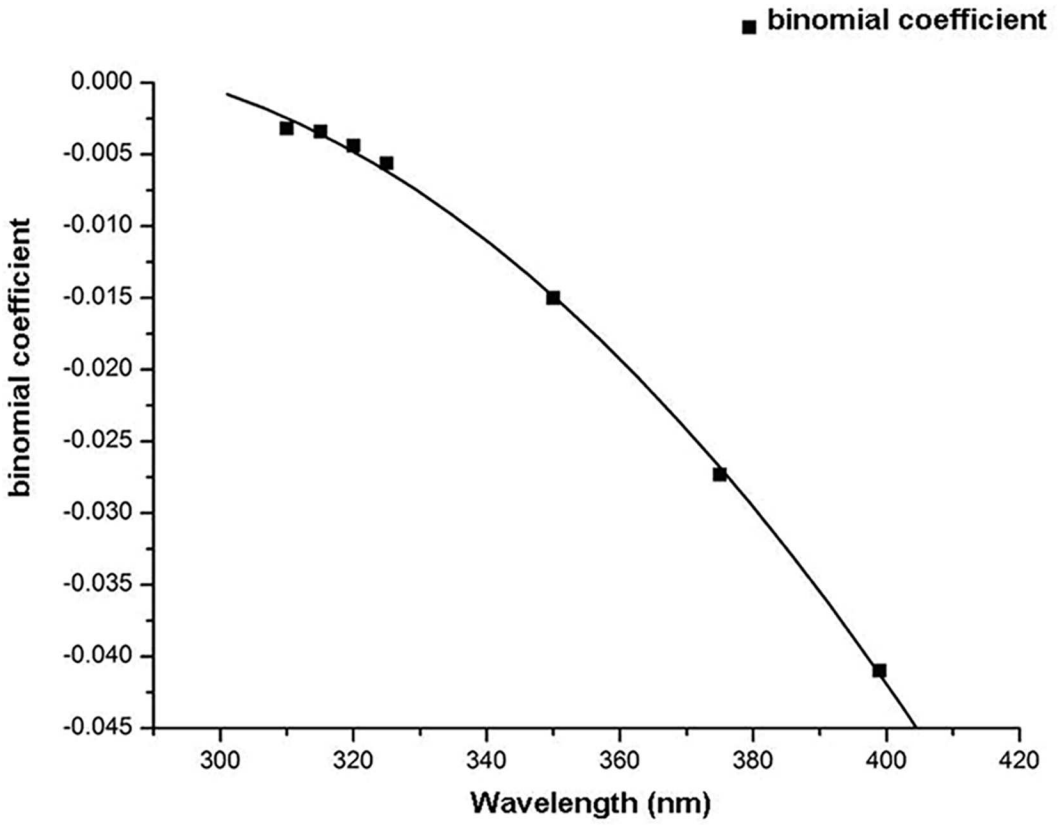

Fig 6. Growth rate of intensity of ocular exposure to reflected UV irradiance with increasing wavelengths and fitted regression curves.

doi:10.1371/journal.pone.0166729.g006

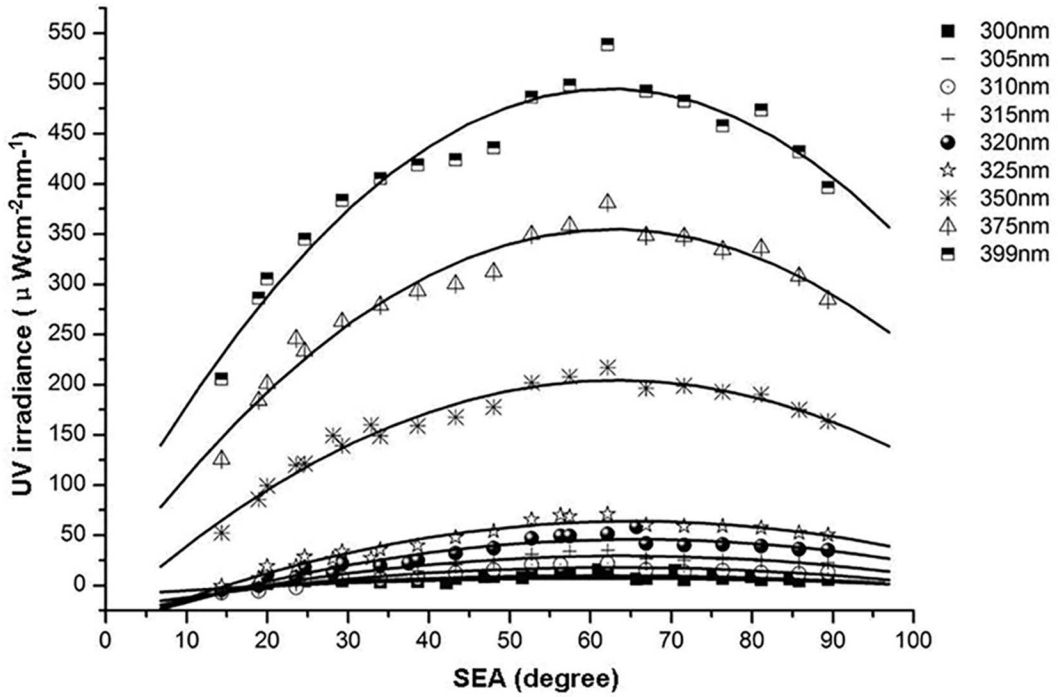

Fig 7. Distributions of intensity of ocular exposure to diffuse UV irradiance of selected wavelengths at different solar elevation angles and fitted regression curves.

doi:10.1371/journal.pone.0166729.g007

Table 3. Fitted equations for distributions of ocular exposure to diffuse UV irradiance of selected wavelengths.

Wavelength (nm)	Fitted equation	R^2
305	y = -0.005x2+0.563x-10.429	R^2 = 0.917
310	y = -0.011x2+1.346x-24.273	R^2 = 0.872
315	y = -0.015x2+1.887x-31.516	R^2 = 0.915
320	y = -0.020x2+2.648x-41.236	R^2 = 0.908
325	y = -0.025x2+3.288x-43.714	R^2 = 0.945
350	y = -0.058x2+7.361x-28.880	R^2 = 0.962
375	y = -0.088x2+11.092x+6.200	R^2 = 0.957
399	y = -0.115x2+14.370x+46.769	R^2 = 0.949

Data represent results for the entire range of solar elevation angles (14–90˚).

doi:10.1371/journal.pone.0166729.t003

exhibited a bimodal distribution [11, 27, 30], in which the ocular exposure to reflected and diffuse UV irradiance contribute to the bimodal distribution of ocular UV exposure. Therefore, it is necessary to study the distributions of direct, reflected, and diffuse irradiance for ocular UV exposure at different solar elevation angles.

In this study, we found that the distributions of ocular exposure to direct UV irradiance values were different from the distributions of ambient UV irradiance values (which were linear in the entire range of solar elevation angles), but the same as distributions of total ocular

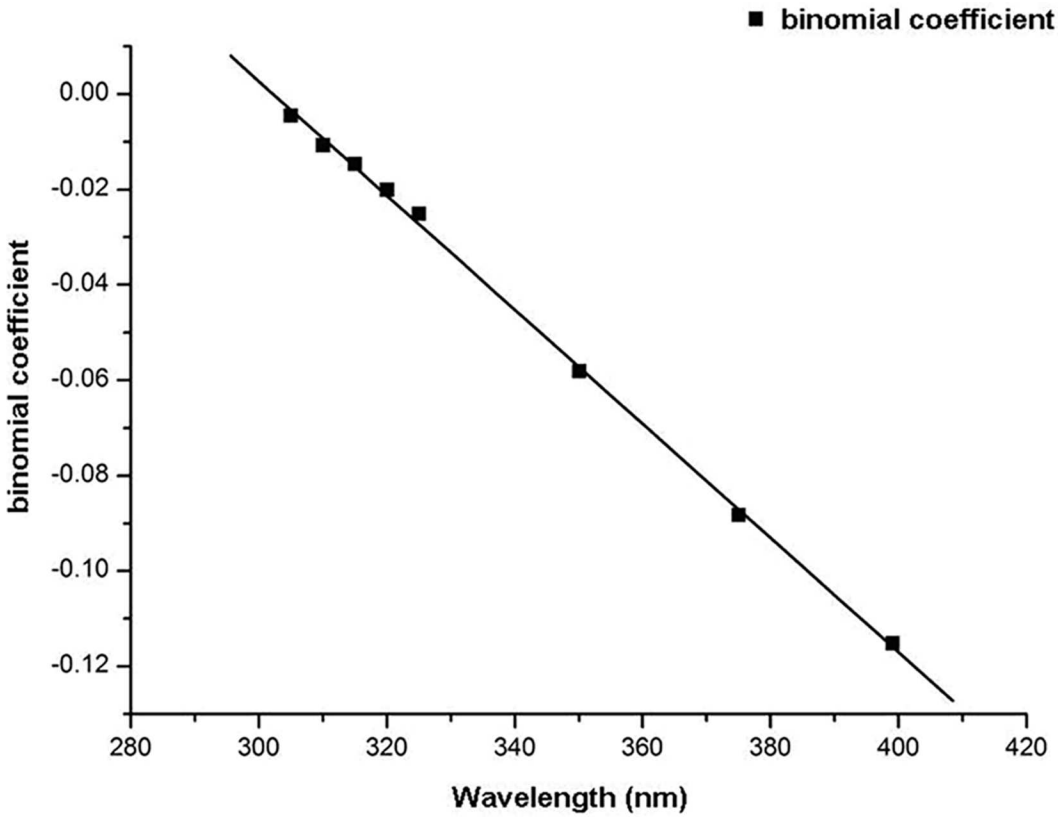

Fig 8. Growth rate of intensity of ocular exposure to diffuse UV irradiance with increasing wavelength and fitted regression curves.

doi:10.1371/journal.pone.0166729.g008

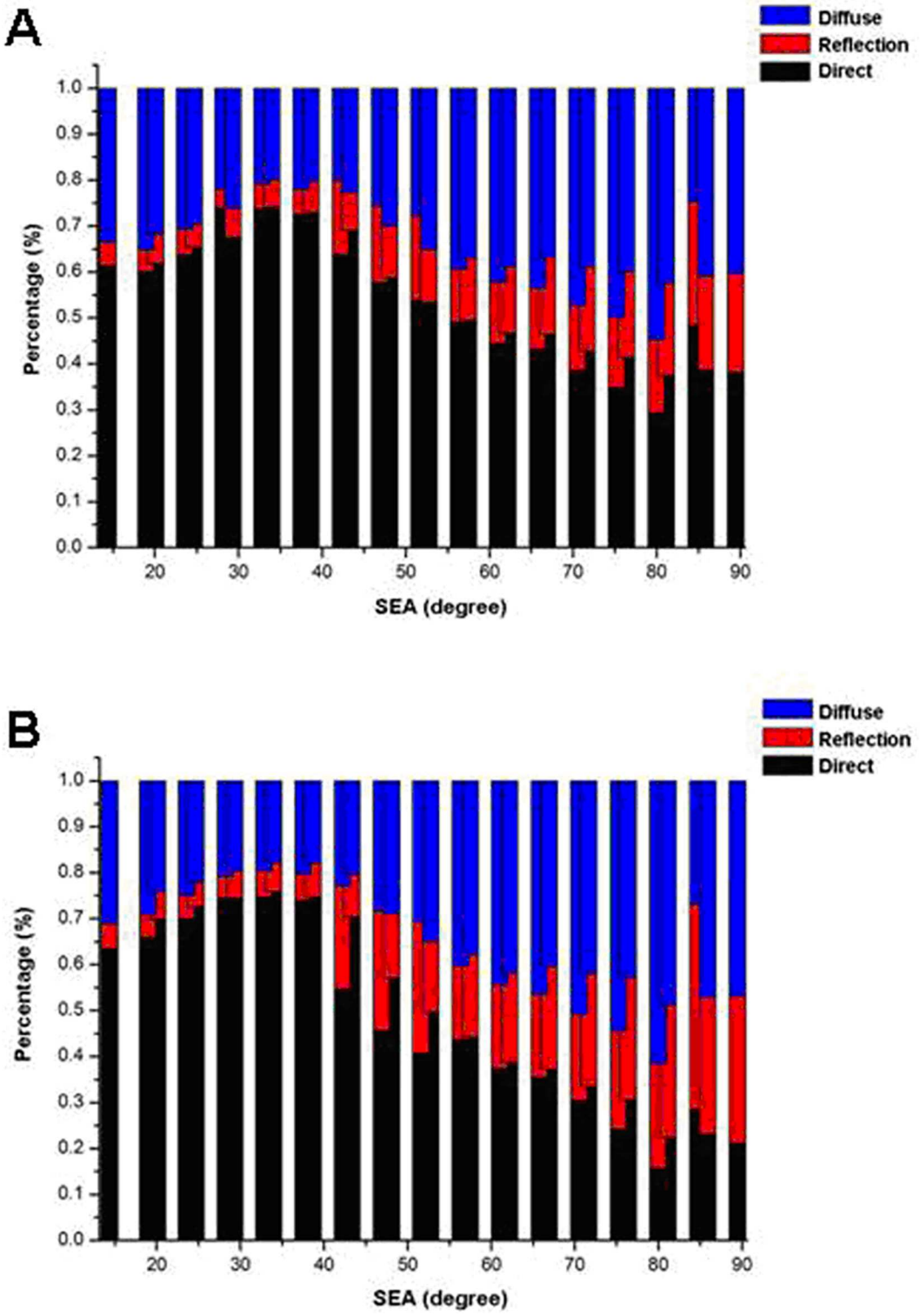

Fig 9. Percentage of total ocular UV exposure due to direct, reflected, and diffuse UV irradiation of 350 nm (A) and 399 nm (B).

doi:10.1371/journal.pone.0166729.g009

exposure to UV irradiation values. Ocular exposure to direct UV irradiance accounted for a large proportion of total ocular exposure to UV irradiation when solar elevation angle was below 50˚. In the high solar elevation angle range (50˚–90˚), ocular exposure to direct UV irradiance decreased with increasing solar elevation angle, but the decreasing trend was significantly faster than that of the total ocular exposure to UV irradiation. One possible reason for this finding is that total ocular exposure to UV irradiation was compensated by the increased impact of ocular exposure to diffuse and reflected UV irradiance.

Distributions of ocular exposure to reflected and diffuse UV irradiance values fit quadratic functions in the entire range of solar elevation angles. The ocular exposure to reflected UV irradiance distribution increased along the entire curve of increasing solar elevation angle, whereas the quadratic curve of ocular exposure to diffuse UV irradiance showed a maximum at about 60˚ solar elevation angle. The increase of ocular exposure to reflected UV irradiance and the magnitude of changes with increasing solar elevation angle were related to the increased ocular exposure to direct UV irradiance and gradual reduction of the incident angle of reflected light. The ocular exposure to diffuse UV irradiance distribution had a quadratic shape, unlike the largely constant intensity of diffuse UV irradiation. Ocular exposure to diffuse UV irradiance first increased and then decreased with increasing solar elevation angle. One reason for this finding may be that the scattering background causes a deviation of the light scattering angle along with the change of solar elevation angle. Another reason may be that diffusion was affected by changes in ambient UV exposure, which would alter the intensity of diffuse UV irradiation to the eyes.

The percentage of ocular exposure to direct UV irradiance in the total ocular exposure to UV irradiation first increased and then decreased with increasing solar elevation angle. For solar elevation angle below 30˚, ocular exposure to direct UV irradiance increased with increasing solar elevation angle, but ocular exposure to reflected and diffuse UV irradiance were less affected. For solar elevation angle above 30˚, ocular exposure to reflected and diffuse UV irradiance increased the amount of UV irradiation incoming to the eyes, whereas the proportion of ocular exposure to direct UV irradiance was lower. This result reaffirms the need to prevent excessive ocular exposure to reflected and diffuse UV irradiation in the higher solar elevation angle range.

This study was performed on a clear, fine day in Sanya city. The measurement site has a relatively unpolluted atmosphere (air pollution index < 50 year round), such that the impact of air pollution was negligible. However, the reflection background was an asphalt surface. Distribution characteristics of ocular exposure to UV irradiation components will be different in snow, water, sand, or other backgrounds. In addition, the meaning of "direct" ocular UV exposure was not the same as the physical concept, but was related to our model monitoring conditions. Overall, the results of this study confirm that eye protection should be used at different times throughout the day because of the different proportions of direct, diffuse, and reflected ocular UV irradiation. The findings also support the construction of mathematical models of ocular UV exposure.

Conclusions

$E_{o,dir}$ distributions were fitted with linear or quadratic functions in different SEA ranges. All $E_{o,refl}$ and $E_{o,diff}$ distributions were fitted with quadratic functions. As SEA increased, the $E_{o,dir}$ portion of E_o increased and then decreased; the $E_{o,refl}$ portion increased from an initial minimum; and the $E_{o,diff}$ portion first decreased and then increased.

Supporting Information

S1 File. Monitored data for ocular UV irradiation.
(DOC)

S2 File. Percentage of direction, reflection and diffusion in total ocular UV irradiation.
(DOC)

Acknowledgments

We thank all the study participants and dedicated personnel.

Author Contributions

Conceptualization: YL.

Data curation: HH.

Formal analysis: JMY HH YL.

Funding acquisition: YL JMY.

Investigation: JMY HH.

Methodology: YL.

Project administration: YL.

Supervision: YL.

Validation: JMY HH YL.

Writing – original draft: JMY.

Writing – review & editing: YL.

References

1. Roberts JE. Ocular phototoxicity. J Photochem Photobiol B. 2001; 64:136–143. PMID: 11744400
2. Cullen AP. Photokeratitis and other phototoxic effects on the cornea and conjunctiva. Int J Toxicol. 2002; 21: 455–464. doi: 10.1080/10915810290169882 PMID: 12537642
3. Boulton M, Rózanowska M, Rózanowski B. Retinal photodamage. J Photochem Photobiol B. 2001; 64:144–161. PMID: 11744401
4. Mesa R, Bassnett S. UV-B-induced DNA damage and repair in the mouse lens. Invest Ophthalmol Vis Sci. 2013 Oct 17; 54(10):6789–97. doi: 10.1167/iovs.13-12644 PMID: 24022010
5. Liou JC, Teng MC, Tsai YS, Lin EC, Chen BY. UV-blocking spectacle lens protects against UV-induced decline of visual performance. Mol Vis. 2015 Aug 6; 21:846–856. PMID: 26283865
6. Newkirk KM, Chandler HL, Parent AE, Young DC, Colitz CM, Wilkie DA, et al. Ultraviolet radiation-induced corneal degeneration in 129 mice. Toxicol Pathol 2007; 35:819–826. doi: 10.1080/01926230701584197 PMID: 17943656
7. Weihs P, Schmalwieser A, Reinisch C, Meraner E, Walisch S, Harald M. Measurements of personal UV exposure on different parts of the body during various activities. Photochem Photobiol. 2013; 89 (4):1004–7. doi: 10.1111/php.12085 PMID: 23587050
8. Sydenham MM, Collins MJ, Hirst LW. Measurement of ultraviolet radiation at the surface of the eye. Invest Ophthalmol Vis Sci. 1997; 38:1485–1492. PMID: 9224276
9. Rosenthal FS, Phoon C, Bakalian AE, Taylor HR. The ocular dose of ultraviolet radiation to outdoor workers. Invest Ophthalmol Vis Sci. 1988; 29:649–656. PMID: 3356520
10. Fleming DP, Walsh JE, Moore LA, Bergmanson JP, McMahon D. A novel sensor array for field based ocular ultraviolet radiation measurements. Radiat Prot Dosimetry. 2006; 118(3):265–74. doi: 10.1093/rpd/nci346 PMID: 16192325
11. Gao N, Hu LW, Gao Q, Ge TT, Wang F, Chu C, et al. Diurnal variation of ocular exposure to solar ultraviolet radiation based on data from a manikin head. Photochem Photobiol. 2012; 88(3):736–43. doi: 10.1111/j.1751-1097.2012.01094.x PMID: 22268421

12. Hu L, Wang F, Ou-Yang NN, Gao N, Gao Q, Ge T, et al. Quantification of ocular biologically effective UV exposure for different rotation angle ranges based on data from a manikin. Photochem Photobiol. 2014; 90(4):925–34. doi: 10.1111/php.12267 PMID: 24588689
13. Oppenrieder A, Hoeppe P, Koepke P. Routine measurement of erythemally effective UV irradiance on inclined surfaces. J Photochem Photobiol B. 2004 May 27; 74(2–3):85–94. doi: 10.1016/j.jphotobiol.2003.11.008 PMID: 15157903
14. Hoeppe P, Oppenrieder A, Erianto C, Koepke P, Reuder J, Seefeldner M, et al. Visualization of UV exposure of the human body based on data from a scanning UV-measuring system. Int J Biometeorol. 2004 Sep; 49(1):18–25. doi: 10.1007/s00484-004-0211-9 PMID: 15232726
15. Kimlin MG, Parisi AV, Downs ND. Human UVA exposures estimated from ambient UVA measurements. Photochem Photobiol Sci. 2003 Apr; 2(4):365–9. PMID: 12760531
16. Streicher JJ, Culverhouse WC Jr, Dulberg MS, Fornaro RJ. Modeling the anatomical distribution of sunlights. Photochem Photobiol. 2004 Jan; 79(1):40–7. PMID: 14974714
17. Weihs P. Influence of ground reflectivity and topography on erythemal UV radiation on inclined planes. Int J Biometeorol. 2002 May; 46(2):95–104. PMID: 12135205
18. Turner J, Parisi AV. Measuring the influence of UV reflection from vertical metal surfaces on humans. Photochem Photobiol Sci. 2009 Jan; 8(1):62–9. doi: 10.1039/b814006e PMID: 19247531
19. Kim J, Cho HK, Mok J, Yoo HD, Cho N. Effects of ozone and aerosol on surface UV radiation variability. J Photochem Photobiol B. 2013; 119:46–51 doi: 10.1016/j.jphotobiol.2012.11.007 PMID: 23334158
20. Pope SJ, Godar DE. Solar UV geometric conversion factors: horizontal plane to cylinder model.PhotochemPhotobiol.2010; 86(2):457–66. doi: 10.1111/j.1751-1097.2009.00679.x PMID: 20059727
21. Baczynska KA, Pearson AJ, O'Hagan JB, Heydenreich J. Effect of altitude on solar UVR and spectral and spatial variations of UV irradiances measured in Wagrain, Austriain winter. Radiat Prot Dosimetry. 2013; 154 (4):497–504. doi: 10.1093/rpd/ncs261 PMID: 23060428
22. Turner J, Parisi AV, Turnbull DJ. Reflected solar radiation from horizontal, vertical and inclined surfaces: ultraviolet and visible spectral and broadband behaviour due to solar zenith angle, orientation and surface type. J Photochem Photobiol B. 2008 Jul 24; 92(1):29–37. doi: 10.1016/j.jphotobiol.2008.03.006 PMID: 18490174
23. Vernez D, Milon A, Vuilleumier L, Bulliard JL.Anatomical exposure patterns of skin to sunlight: relative contributions of direct, diffuse and reflected ultraviolet radiation. Br J Dermatol. 2012; 167(2):383–90. doi: 10.1111/j.1365-2133.2012.10898.x PMID: 22356161
24. Garrison LM, Murray LE, Doda DD, Green AE. Diffuse-direct ultraviolet ratios with a compact double monochromator. Appl Opt. 1978; 17 (5):827–36. doi: 10.1364/AO.17.000827 PMID: 20197880
25. Vernez D, Milon A, Francioli L, Bulliard JL, Vuilleumier L, Moccozet L.A numeric model to simulate solar individual ultraviolet exposure. Photochemistry and Photobiology, 2011, 87: 721–728 doi: 10.1111/j.1751-1097.2011.00895.x PMID: 21223287
26. Parisi AV, Kimlin MG, Lester R, Turnbull D.Lower body anatomical distribution of solar ultraviolet radiation on the human form in standing and sitting postures. J Photochem Photobiol B. 2003: 69(1):1–6. PMID: 12547490
27. Wang F, Gao Q, Hu L, Gao N, Ge T, Yu J, Liu Y.Risk of eye damage from the wavelength-dependent biologically effective UVB spectrum irradiances. PLoS One. 2012; 7(12):e52259. doi: 10.1371/journal.pone.0052259 PMID: 23284960
28. Liu GC, Wang F, Gao YY, Yang Z, Hu LW, Gao Q, et al. The enhancement of biological ocular UV radiation on beaches compared to the radiation on grass. J Photochem Photobiol B. 2014; 141:106–12. doi: 10.1016/j.jphotobiol.2014.09.009 PMID: 25463657
29. Serrano D, Mar´ın MJ, Utrillas MP, Tena F, Mart´ınez-Lozano JA.Measurement and modelling of global erythemal irradiance on inclined planes. Tethys. 2010; 7: 57–66
30. Hu LW, Gao Q, Gao N, Liu G, Wang Y, Gong HZ, et al. Solar UV exposure at eye is different from environmental UV: diurnal monitoring at different rotation angles using a manikin. J. Occup. Environ. Hyg. 2013; 10(1):17–25. doi: 10.1080/15459624.2012.737700 PMID: 23145494